Myelin imaging

van der Weijden, Kars

DOI:
10.33612/diss.262505423

Chapter 4

The effect of lesion filling on brain network analysis in multiple sclerosis using structural magnetic resonance imaging

Chris W.J. van der Weijden[1]*, Milena S. Pitombeira[2]*, Yudith R.A. Haveman[1], Carlos A. Sanchez-Catasus[1,4], Kenia R. Campanholo[3], Guilherme D. Kolinger[1], Carolina M. Rimkus[3], Carlos Alberto Buchpiguel[3], Rudi A.J.O. Dierckx[1], Remco J. Renken[5], Jan F. Meilof[6,7], Erik F.J. de Vries[1], Daniele de Paula Faria[3]

[1]Department of Nuclear Medicine and Molecular Imaging, University of Groningen, University Medical Center Groningen, Hanzeplein 1, Groningen, The Netherlands
[2]Department of Neurology, Faculdade de Medicina da Universidade de Sao Paulo, Sao Paulo, Brazil
[3]Department of Radiology and Oncology, Faculdade de Medicina da Universidade de Sao Paulo, Sao Paulo, Brazil
[4]Department of Neurology, Clínica Universidad de Navarra, 31008 Pamplona, Spain
[5]Department of Neuroscience, University Medical Center Groningen, University of Groningen, Hanzeplein 1, Groningen, The Netherlands
[6]Department of Biomedical Sciences of Cells and Systems, University of Groningen, University Medical Center Groningen, Hanzeplein 1, Groningen, The Netherlands
[7]Department of Neurology, Martini Ziekenhuis, Groningen, The Netherlands

Published in: Insights into Imaging, 28 March 2022, Volume 13, Article number 63, https://doi.org/10.1186/s13244-022-01198-4

4.1. Abstract

Introduction

Graph theoretical network analysis with structural magnetic resonance imaging (MRI) of multiple sclerosis (MS) patients can be used to assess subtle changes in brain networks. However, the presence of multiple focal brain lesions might impair the accuracy of automatic tissue segmentation methods, and hamper the performance of graph theoretical network analysis. Applying "lesion filling" by substituting the voxel intensities of a lesion with the voxel intensities of nearby voxels, thus creating an image devoid of lesions, might improve segmentation and graph theoretical network analysis. This study aims to determine if brain networks are different between MS subtypes and healthy controls (HC) and if the assessment of these differences is affected by lesion filling.

Methods

The study included 49 MS patients and 19 HC that underwent a T_1w, and T_2w-FLAIR MRI scan. Graph theoretical network analysis was performed from grey matter fractions extracted from the original T_1w-images and T_1w-images after lesion filling.

Results

Artefacts in lesion-filled T_1w images correlated positively with total lesion volume ($r=0.84$, $p<0.001$), and had a major impact on grey matter segmentation accuracy. Differences in sensitivity for network alterations were observed between original T_1w data and after application of lesion filling: Graph theoretical network analysis obtained from lesion-filled T_1w images produced more differences in network organization in MS patients.

Conclusion

Lesion filling might reduce variability across subjects resulting in an increased detection rate of network alterations in MS, but also induces significant artefacts, and therefore should be applied cautiously especially in individuals with higher lesions loads.

4.2. Introduction

Multiple sclerosis (MS) is an inflammatory demyelinating disease, and the most common neurodegenerative disease among young adults.[1] The disease is characterized by apparently randomly located inflammatory lesions within the central nervous system (CNS), resulting in a variety of clinical manifestations among patients.[1] The relapsing-

remitting multiple sclerosis phenotype (RRMS) presents acute clinical manifestations, the so-called relapses, followed by a period of full or partial recovery and stable disability between episodes, whereas the progressive phenotype (PMS) is defined when a consistent increasing in neurological disability is confirmed independent of relapses.[4,5,417,418] Despite the high heterogeneity within MS pathology due to the random location of lesions, there are also common symptoms. These symptoms may include a decreased visual function, bladder dysfunction, and impaired motor and sensory functions.[419] Although allocation of symptoms to specific spinal cord dysfunction is generally supported by a myelopathy visible on MRI, studies have not yet been able to consistently link symptoms to individual cerebral lesions visible on MRI. A general explanation for this discrepancy is the existence of functional cerebral networks, which implies that lesions in different parts of a network can result in similar symptoms. A progressive disruption of functional networks during disease progression could explain the increase in disability in later stages of MS.

To investigate this hypothesis, graph theoretical network analysis could be used for different phenotypes or stages of MS. According to graph theory, the connections between brain regions can be presented in a graph, in which the brain regions are represented as nodes and the interactions as lines (edges). These interactions can be used to calculate various parameters, like path length, which describes the number of edges between two brain regions. These parameters are calculated per subject and can then be compared between two groups. In principle, any imaging modality could be used for graph theory, but the clinical meaning and relevance is highly depending on the imaging used as input. So far, mainly diffusion tensor imaging (DTI) has been used for structural network analysis in MS.[420] DTI assesses white matter (WM) tractography and therefore could be used to determine white matter connectivity. Grey matter (GM) connectivity in MS could be studied using parameters obtained from T_1-weighted (T_1w) MRI, such as cortical volume, cortical thickness, or grey matter fraction.[420] Studies showed high similarities between DTI and T_1w results obtained with graph theoretical network analysis in MS patients.[421–423] A challenge for network analysis using either DTI or T_1w MRI in MS is the random location of lesions, and for T_1w especially the effect of juxtacortical lesions on GM segmentation. A method to cope with the variation in lesion load and distribution is the application of lesion filling.[424] Lesion filling replaces the voxel intensities in lesions with the voxel intensity of surrounding tissue, resulting in an image without apparent lesions, and thus devoid of the pathological signal intensity variations. Some studies performing network analysis in MS apply lesion filling,[425,426] whereas others do not,[421,427] and therefore there is no clear consensus regarding the application of lesion filling.

Studies on structural networks using graph theoretical network analysis in MS show

inconsistent findings. Some studies, assessing either GM (T_1w) or WM (DTI) connectivity, found a decrease in global and local efficiency of the network in MS patients,[421–423,428] whereas other studies found an increase.[425,427,429] This discrepancy between studies might reflect the deteriorating reorganizational properties of the brain to minimise clinical disability during disease progression. These controversies regarding WM and GM connectivity could therefore be due to differences in study populations, especially with regard to disease duration and disease subtype. Dedicated studies on the effects of different MS phenotypes or disease stages on connectivity measures could help to resolve this issue.

Our study aims to 1) determine the effect of lesion filling on graph theoretical network parameters derived from T_1w MRI, 2) identify which regions are important for MS pathogenesis by assessing abnormalities in GM connectivity, and 3) investigate if GM connectivity differs between RRMS and PMS patients.

4.3. Methods

4.3.1. Participants

Seventy-five subjects were recruited at the Medical Faculty of the University of São Paulo, which consisted of 24 healthy controls (HC), 30 RRMS patients, and 21 PMS patients. Inclusion criteria for the healthy controls were age between 18 and 65 years and at least 4 years of education. Patients were diagnosed with clinically defined MS according to the revised McDonald criteria,[374] were relapse free and had not received steroid treatment for at least 30 days before MRI scanning. Exclusion criteria were any major medical conditions that prevented MRI acquisition (i.e. pregnancy, renal, cardiac, or hepatic insufficiency) or presence of severe psychiatric disorders. Hence, 3 healthy subjects were excluded due to unexpected comorbidities, 1 participant withdrew from the study and did not allow further use of data, 1 participant was scanned with a different head coil due to dysphagia, 1 subject did not conclude the whole protocol, and 1 participant received intravenous steroid treatment 5 days before MRI acquisition which was reported only after the scan. All participants signed the informed consent form to participate in the study. The study was conducted according to the Declaration of Helsinki and subsequent revisions, and was approved by the medical ethics committee of the University of São Paulo (protocol 3.256.558). Differences in demographics were assessed with non-parametric tests where applicable.

4.3.2. Image acquisition

MRI scans of the brain were performed on a 3T SIGNA PET-MRI scanner (General Electric Company) with a 24-channel head coil. The protocol comprised of a 3D-T_1w (TR/TE/TI = 7.664/3.112/600 ms, voxel size 1x0.5x0.5mm) and a 3D- T_2w FLAIR (TR/TE/TI = 6500/141.213/1905 ms, voxel size 1.3x0.5x0.5 mm)sequence.

4.3.3. Image processing

T_2w-FLAIR images were co-registered to the 3D-T_1w images. The lesion growth algorithm (LGA) of the lesion segmentation toolbox (LST) in SPM12 (Wellcome Trust Centre for Neuroimaging, Institute of Neurology, London, 2014) was used with a kappa of 0.3 to perform lesion segmentation on T_1w and T_2w-FLAIR images, resulting in a lesion probability map. Subsequently, these lesion probability maps were used for lesion filling of T_1w images by using local information (i.e. filling the lesion with the intensity of adjacent voxels), allowing accurate lesion filling even in images that are corrupted by bias field.[430] Original and lesion-filled T_1w MRI images were processed by GM, WM and cerebrospinal fluid (CSF) segmentation and spatial normalization to the Montreal Neurological Institute (MNI) space using the tissue probability maps in SPM12.[370] The accuracy of the co-registration, segmentation, lesion filling, and normalisation was checked by visual inspection. Network analysis was performed both on the original T_1w data and on the T_1w data with lesion filling.

4.3.3. Network-analysis

Graph theoretical network analysis comprises 4 main steps (Figure 4.1): 1) defining the appropriate nodes, 2) estimation of a continuous measure of association between nodes, 3) generation of an association matrix, and 4) calculating the network parameters of interest. Using the 116 regions of interest (ROIs) within the automated anatomical labelling (AAL) atlas within the Wake Forest University (WFU) pickatlas tool in SPM12,[431] grey matter fractions were extracted from the GM segmentation derived of ROIs in the T_1w images. The grey matter fractions corresponding to the 116 AAL ROIs were used as nodes. Association matrices were generated with Brain Analysis using Graph theory (BRAPH)[432] from Spearman correlations to assess the inter-regional associations (the edges between nodes): a higher correlation indicated a stronger inter-region association. Spearman correlations were used due to their insensitivity to outliers and skewed distributions. Negative correlations were set to zero, because not all network parameters can be calculated in the presence of negative correlation coefficients. In recent years there have been advances in using weighted graphs and increasing calls for their use across all neuroimaging modalities.[433] Therefore, several network parameters (Table 4.1) were calculated per group using weighted undirected

Table 4.1: *Studied network parameters and their definitions*

Measure	Definition	Nodal level	Global level
degree	number of connections to a node	x	x*
strength	sum of the weight of all connections to a node	x	x*
path length	lowest number of connections between two nodes	x	x*
clustering coefficient	the fraction of a node's neighbours that are also neighbour between each other	x	x*
global efficiency	average inverse of shortest path length	x	x*
local efficiency	global efficiency of a node regarding its neighbourhood	x	x*
Within module degree z-score	within module degree of centrality	x	
Participation	the diversity of intermodular interconnections of individual nodes	x	
transitivity	the probability of interconnectivity of adjacent nodes		x
modularity	degree to which the graph can be subdivided into multiple small-world networks		x
assortativity coefficient	correlation coefficient between degrees/strengths of all nodes on two opposite ends of a connection		x
small-worldness	The ratio of clustering coefficient on global level and the clustering coefficient of a random graph divided by the ratio of the average path length on global level and the average path length of a random graph		x

** Network parameters at global level were calculated by averaging the outcome of nodal measures over all ROI's*

graphs. Global parameters are calculated over the whole brain and therefore provide information regarding the integrity of the whole brain network. However, nodal parameters are calculated for individual brain regions, and thus provide information regarding the network integrity of the individual brain regions.

Non-parametric permutation tests were applied to both data derived from original T_1w MRI and data derived from lesion filled T_1w MRI to assess the significance of the differences in the network parameters between two groups (HC vs. MS total, HC vs. RRMS, HC vs. PMS, and RRMS vs. PMS).[434] The tests were performed by first determining the differences between two groups for each network parameter. Then, the subjects were permutated between the two groups and the network parameters (e.g. strength) were calculated again for the permuted groups (containing a mix of subjects of the two groups). This process was repeated 1000 times. After each permutation, the differences in network parameters between the permutated groups were determined, resulting in distributions of between-group differences and 95% confidence intervals (CIs) of the differences per network parameter. HC (or RRMS in case of RRMS vs. PMS) were used as a reference for the 95% CIs. If the distribution of a particular MS group was outside the 95% CI of the reference group (HC or RRMS), the difference was considered significant

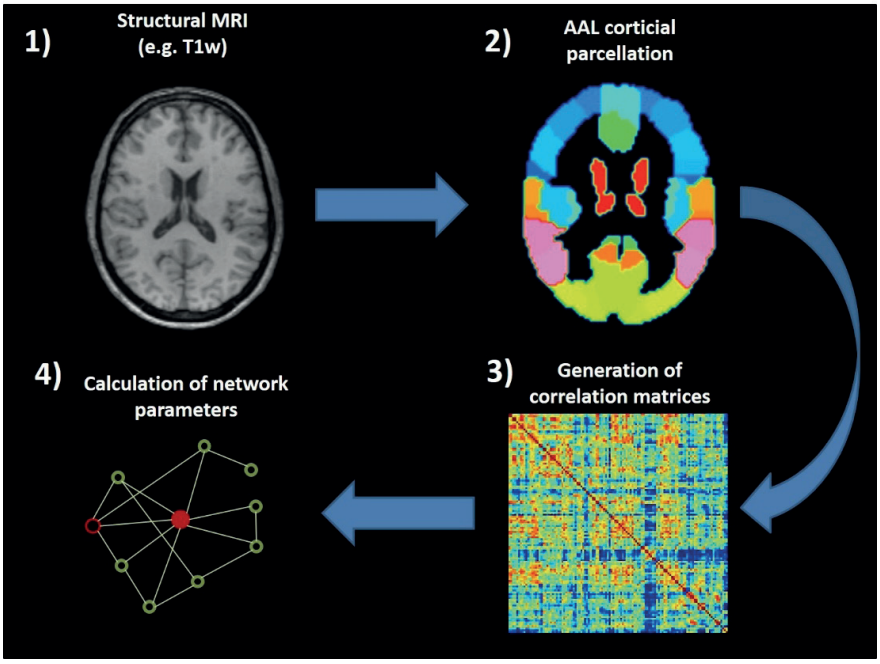

Figure 4.1: *Flowchart of the graph theoretical network analysis. AAL = automated anatomical labelling*

at a global level. The results on a nodal level were corrected for multiple comparisons using the false discovery rate (FDR) Benjamini Hochberg procedure[435] with a q of 0.05 to correct for the number of regions that were tested. Differences were considered to be truly significant and not dependent on chance, if the uncorrected p-values were both ≤0.05 and equal to or smaller than the FDR corrected p-values.

4.4. Results

4.4.1. Study population

Only patients off-steroid treatment without comorbidities, who correctly concluded the whole MRI protocol, were included in the graph theoretical network analysis. This led to a final inclusion of 19 HC, 30 RRMS (disease duration 9.3y ±5.9), and 19 PMS patients (disease duration 11.8y ±6.8), of which 11 had primary and 8 secondary PMS (Table 4.2). Patients with RRMS were significantly younger (age 35.7 vs. 49.3 y, t=-5.7, p<0.001) and had significantly lower disability scores than PMS patients (EDSS 2.7 vs 6.3, U=556, p<0.001), but had similar numbers and volumes of white matter lesions, years of education, and disease duration. Surprisingly, a small number of non-

specific brain lesions that do not correspond with a specific diagnosis or aetiology were detected in HC.

Table 4.2: *Study population characteristics. Age, Education, Disease duration, EDSS, Amount of lesions, Lesion volume are presented as mean (±SD). Significant differences between RRMS and PMS patients are indicated with an asterisk. * p<0.001.*

	HC	MS total	RRMS	PMS
Number of paticipants	19	49	30	19
Gender (%male)	21.1	34.7	29.0	42.1
Age (y)	41.3 (±12.8)	41.0 (±10.5)	**35.7 (±7.6)***	**49.3 (±8.9)***
Education (y)	13.9 (±3.8)	13.1 (±3.9)	13.7 (±3.5)	12.3 (±4.4)
Disease duration (y)	0	10.3 (±6.3)	9.3 (±5.9)	11.8 (±6.8)
EDSS	0 (±0)	4.1 (±2.1)	**2.7 (±1.4)***	**6.3 (±0.8)***
Number of lesions	1.9 (±2.7)	15.7 (±8.5)	16.3 (±9.3)	14.7 (±7.3)
Total lesion volume (ml)	0.3 (±0.8)	23.9 (±8.5)	15.3 (±18.7)	25.5 (±29.9)

4.4.2. Global network topology based on original T_1w MRI data

Modularity and assortativity were the only global network parameters derived from T_1w images without lesion filling that showed significant differences between groups. Modularity was significantly higher in HC than in MS patients. The T_1w-derived assortativity (correlation coefficient, indicating whether similar nodes are connected to each other) was significantly lower in HC than in MS patients (Table 4.3, Figure 4.2). Both parameters did not significantly differ between RRMS and PMS patients.

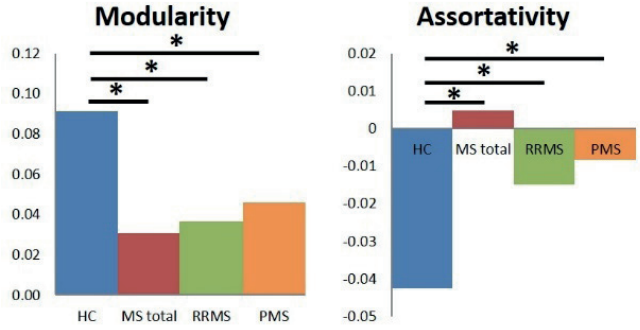

Figure 4.2: *Group differences of T_1w MRI data without lesion filling in the global graph theoretical network parameters modularity and assortativity. Comparisons were made for HC vs. MS total, HC vs. RRMS, HC vs. PMS, and RRMS vs. PMS. Significant differences are indicated with an asterisk *.*

4.4.3. Lesion filling

Lesion filling on T_1w MRI data was applied to evaluate the effect of lesion filling on the graph theoretical network outcome parameters. In total 804 lesions were detected across the study population. Lesion-filling was accompanied with a total amount of 233 artefacts, of which 79 were substantial (wrong classification of tissue) and 152 minor (Figure 4.3). Most artefacts generated by lesion filling were observed for lesions at the interface between tissues (e.g. interface between WM and CSF, or WM and GM) and lesions with a large volume. Quantitative assessment using Spearman correlation, revealed a correlation between total lesion volume and the number of lesion filling artefacts ($r=0.84$, $p<0.001$). An example of the substantial effects of the lesion filling artefacts on GM segmentations is displayed in Figure 4.4. All images were included in the network analysis, irrespective of the extent of lesion filling artefacts.

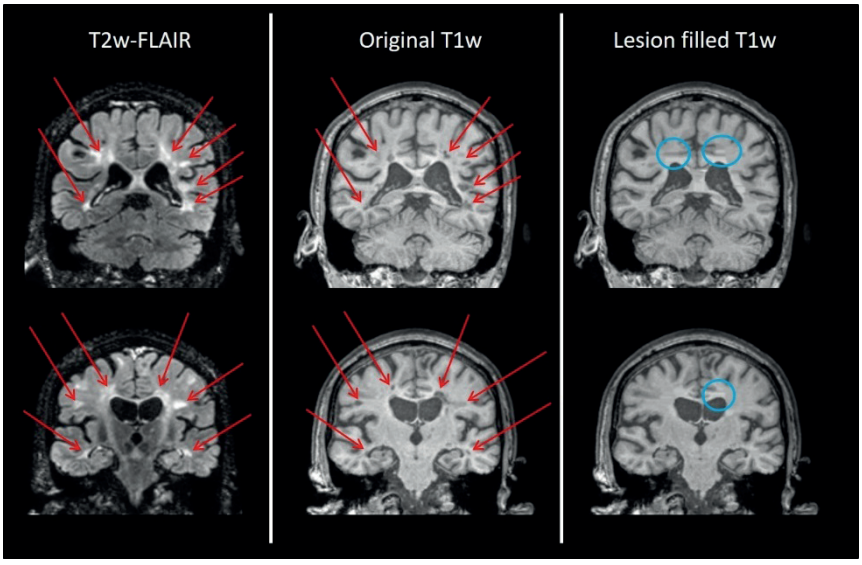

Figure 4.3: *The effects of lesion filling on T_1w MRI illustrating artefacts due to lesion filling. Red arrows depict the locations of the lesions; blue circles depict lesion filling artefacts. The upper row shows some substantial artefacts due to lesion filling, composed of grey matter tissue allocation in the middle of white matter regions, the lower row shows a minor artefact, having blunt white matter edges.*

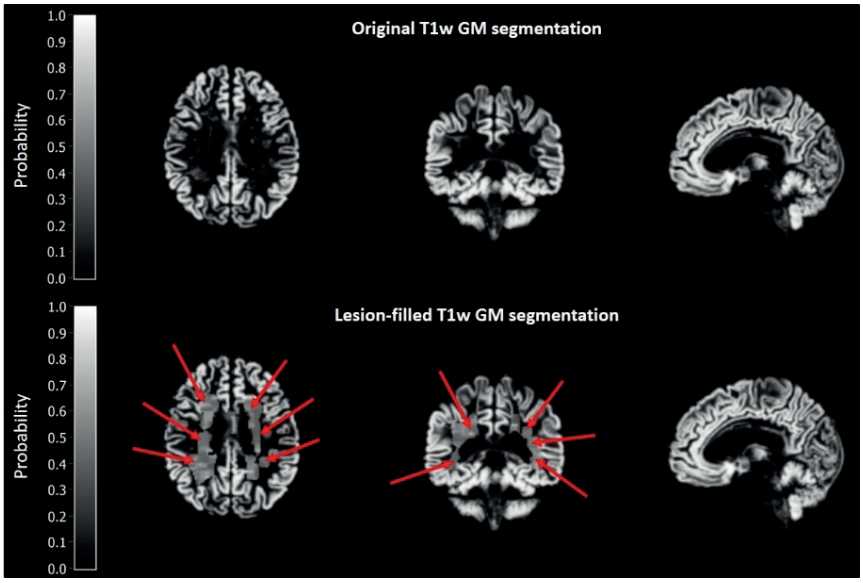

Figure 4.4: *GM segmentation of both original T_1w and lesion-filled T_1w MRI*

4.4.4. Global network topology of lesion filled MRI

Network analysis of lesion-filled T_1w images (Figure 4.5 & Table 4.3) showed significant differences in all global network parameters between the HC and total MS group. In particular, the average degree, average strength, global and local efficiency, clustering coefficient, transitivity, assortativity, and small-worldness were significantly increased in the total MS group, whereas the average path-length and modularity were significantly decreased (Table 4.3). Comparison of HC with RRMS showed similar significant differences for all parameters. The PMS group only significantly differed from HC for the parameters average degree, average strength, transitivity, path-length and modularity. For all network parameters, the scores of the PMS group deviated less from HC than those of the RRMS group. No statistically significant differences between the RRMS and PMS group were found for any of the parameters.

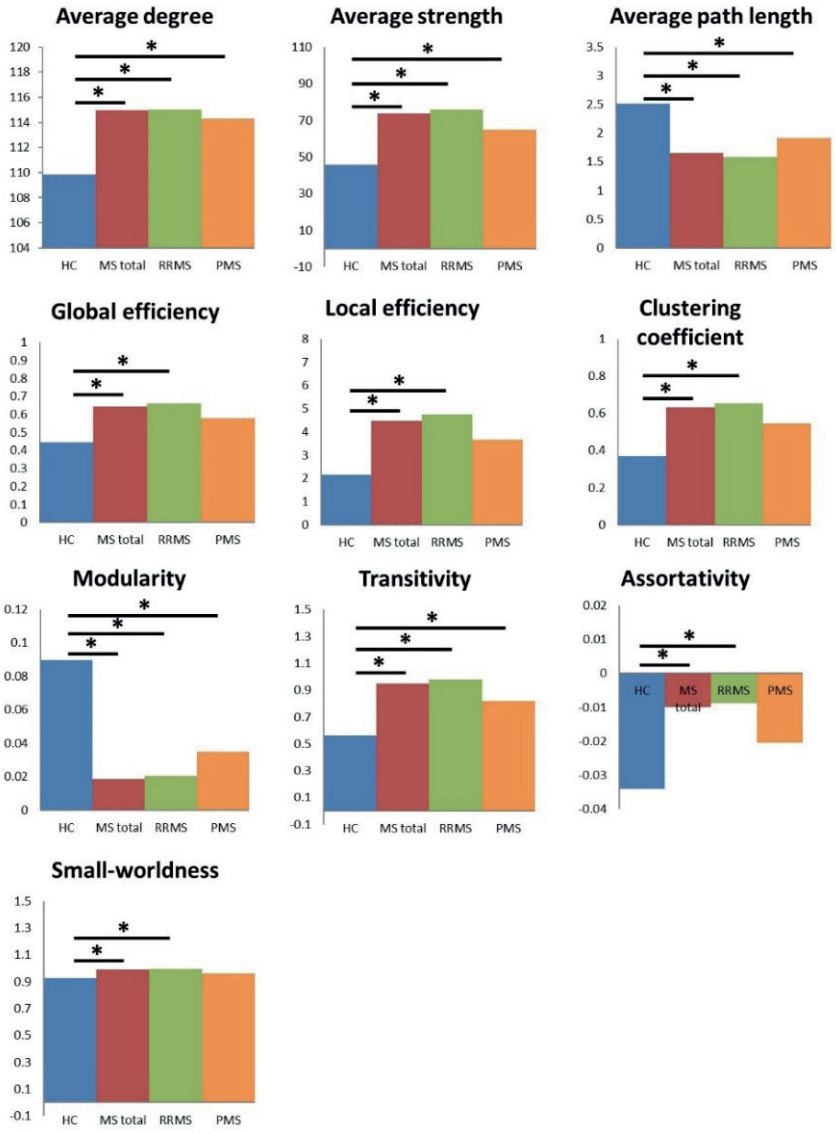

Figure 4.5: *Group differences using lesion filled T_1w data in global graph theoretical network parameters of structural connectomes. Comparisons that have been made were HC vs. MS total, HC vs. RRMS, HC vs. PMS, and RRMS vs. PMS. Significant differences are indicated with an asterisk *.*

Table 4.3: *Differences in global graph theoretical network parameters between groups. The corresponding 95% confidence intervals (CI) are presented between brackets.*

Network parameter	MRI	HC vs. MS total	HC vs. RRMS	HC vs. PMS	RRMS vs. PMS
Average degree	Original T_1w	3.17 (-1.35 – 7.37)	3.93 (-2.68 – 7.60)	0.29 (-4.50 – 4.61)	-3.64 (-6.50 – 3.59)
	Lesion-filled T_1w	**5.16 (-0.01 – 2.31)***	**5.17 (-0.38 – 2.68)***	**4.48 (-1.93 – 1.80)***	-0.69 (-2.07 – 0.29)
Average strength	Original T_1w	17.0 (-17.2 – 21.4)	16.0 (-21.0 – 23.1)	14.5 (-21.5 – 21.8)	-1.5 (-23.0 – 19.9)
	Lesion-filled T_1w	**27.9 (-15.0 – 20.0)***	**30.1 (-20.4 – 23.4)***	**19.0 (-18.1 – 18.5)***	-11.1 (-20.3 – 17.7)
Average path length	Original T_1w	-0.46 (-0.66 – 0.53)	-0.46 (-0.75 – 0.67)	-0.40 (-0.64 – 0.60)	0.06 (-0.63 – 0.64)
	Lesion-filled T_1w	**-0.86 (-0.57 – 0.34)***	**-0.92 (-0.63 – 0.54)***	**-0.60 (-0.49 – 0.46)***	0.32 (-0.48 – 0.55)
Global efficiency	Original T_1w	0.11 (-0.14 - 0.14)	0.10 (-0.16 – 0.15)	0.10 (-0.16 – 0.16)	0.00 (-0.15 – 0.17)
	Lesion-filled T_1w	**0.20 (-0.12 – 0.15)***	**0.22 (-0.17 – 0.18)***	0.13 (-0.14 – 0.14)	-0.08 (-0.15 – 0.14)
Local efficiency	Original T_1w	1.26 (-1.91 – 1.78)	1.16 (-1.91 – 1.72)	1.22 (-1.93 – 2.00)	0.06 (-1.66 – 2.01)
	Lesion-filled T_1w	**2.33 (-1.68 – 2.01)***	**2.60 (-2.29 – 2.26)***	1.50 (-1.91 – 2.14)	-1.10 (-2.15 – 2.00)
Clustering	Original T_1w	0.17 (-0.14 – 0.19)	0.15 (-0.18 – 0.20)	0.14 (-0.20 – 0.19)	-0.01 (-0.19 – 0.17)
	Lesion-filled T_1w	**0.26 (-0.12 – 0.19)***	**0.28 (-0.19 – 0.21)***	0.17 (-0.17 – 0.17)	-0.11 (-0.20 – 0.15)
Transitivity	Original T_1w	0.25 (-0.22 – 0.30)	0.22 (-0.27 – 0.29)	0.22 (-0.28 – 0.30)	0.00 (-0.31 – 0.26)
	Lesion-filled T_1w	**0.39 (-0.19 – 0.27)***	**0.42 (-0.26 – 0.34)***	0.26 (-0.24 – 0.26)	-0.16 (-0.30 – 0.22)
Modularity	Original T_1w	**-0.061 (-0.060 – 0.014)***	**-0.055 (-0.054 – 0.030)***	**-0.045 (-0.040 – 0.038)***	0.010 (-0.029 – 0.054)
	Lesion-filled T_1w	**-0.071 (-0.044 – 0.011)***	**-0.069 (-0.050 – 0.028)***	**-0.054 (-0.026 – 0.027)***	0.015 (-0.017 – 0.039)
Assortativity	Original T_1w	**0.047 (-0.024 – 0.031)***	**0.028 (-0.022 – 0.025)***	**0.034 (-0.027 – 0.026)***	0.007 (-0.051 – 0.048)
	Lesion-filled T_1w	**0.024 (-0.001 – 0.023)***	**0.025 (-0.008 – 0.024)***	0.014 (-0.019 – 0.019)	-0.012 (-0.018 – 0.008)
Small-worldness	Original T_1w	0.010 (-0.027-0.064)	0.019 (-0.038-0.064)	-0.011 (-0.048-0.051)	-0.030 (-0.060-0.053)
	Lesion-filled T_1w	**0.065 (-0.011-0.056)***	**0.069 (-0.028-0.054)***	0.034 (-0.039-0.041)	-0.035 (-0.053-0.027)

*Differences relative the healthy controls are statistically significant when the differences fall outside the 95% CI. Significant differences are indicated with an asterisk *. No statistically significant differences were observed between the RRMS and PMS group.*

4.4.5. Nodal network topology with and without lesion filling

Regional values for nodal network topology are presented in appendix table 4.1-4.6. For a better overview, FDR corrected significant nodes (q=0.05) were compiled together based on their anatomical location (Table 4.4). When assessing network parameters derived from original MRI data at the level of individual nodes, the

Table 4.4: *Compilation of regional differences in network topology derived from lesion-filled T_1w MRI images. The results for the comparisons of the different MS groups with healthy controls are provided. The comparison RRMS vs. PMS did not yield any significant results.*

	MS group	Frontal lobe	Temporal lobe	Parietal lobe	Occipital lobe	Central structures	Cingulate gyri	Posterior fossa
Path length	MS total	↓	↓	↓	↓	n.s.	↓	↓
	RRMS	↓	↓	↓	↓	n.s.	↓	↓
	PMS	n.s.	↓	↓	↓	n.s.	n.s.	↓
Degree	MS total	↑	↑	↑	↑	↑	↑	↑
	RRMS	↑	↑	↑	↑	↑	↑	↑
	PMS	↑	↑	↑	↑	↑	↑	↑
Strength	MS total	↑	↑	↑	↑	n.s.	↑	↑
	RRMS	↑	↑	n.s.	n.s.	n.s.	n.s.	↑
	PMS	n.s.	n.s.	n.s.	n.s.	n.s.	n.s.	n.s.
Global efficiency	MS total	n.s.	n.s.	n.s.	n.s.	n.s.	n.s.	↑
	RRMS	n.s.	n.s.	n.s.	n.s.	n.s.	n.s.	↑
	PMS	n.s.	n.s.	n.s.	n.s.	n.s.	n.s.	n.s.
Local efficiency	MS total	n.s.	n.s.	n.s.	n.s.	n.s.	n.s.	n.s.
	RRMS	n.s.	n.s.	n.s.	n.s.	n.s.	n.s.	n.s.
	PMS	n.s.	n.s.	n.s.	n.s.	n.s.	n.s.	n.s.
Clustering	MS total	↑	↑	↑	↑	n.s.	↑	↑
	RRMS	n.s.	n.s.	n.s.	n.s.	n.s.	n.s.	↑
	PMS	n.s.	n.s.	n.s.	n.s.	n.s.	n.s.	n.s.
Within module degree z-score	MS total	n.s.	n.s.	n.s.	n.s.	n.s.	n.s.	n.s.
	RRMS	n.s.	n.s.	n.s.	n.s.	n.s.	n.s.	n.s.
	PMS	n.s.	n.s.	n.s.	n.s.	n.s.	n.s.	n.s.
Participiation	MS total	n.s.	n.s.	n.s.	n.s.	n.s.	n.s.	n.s.
	RRMS	n.s.	n.s.	n.s.	n.s.	n.s.	n.s.	n.s.
	PMS	n.s.	n.s.	n.s.	n.s.	n.s.	n.s.	n.s.

** n.s. = not significant, ↑ is significantly increased compared to HC, ↓ is significantly decreased compared to HC*

degree was statistically significant decreased in frontal lobe of PMS compared to HC, and increased in posterior fossa of PMS compared to HC (Appendix table 4.1). No significant differences between groups were observed for any other parameter after false-discovery rate (FDR) correction. In contrast, network analysis of lesion-filled T_1w images showed statistically significant differences between groups for many regional

network topologies, even after FDR correction (Table 4.4 and Appendix table 4.2-4.6).

The nodal degree was increased in all brain areas in all MS groups, when compared to HC. Nodal strength, global efficiency, and cluster coefficient in posterior fossa was higher in the total MS and RRMS groups than in HC, but was not affected in PMS. In all MS groups, path length in the temporal lobe, parietal lobe, occipital lobe, and posterior fossa was lower than in HC. In the total MS and RRMS groups, path length was also decreased in the frontal lobe and in the insula and cingulate gyri.

Assessing the regions more in detail (Appendix table 4.2-4.6), most network parameters were affected in the right Heschl gyrus, cerebellum crus 2, and right cerebellum part 7b in all MS groups, whereas nodal degree, nodal strength, path length, and clustering coefficient were also affected in right superior occipital gyrus, and left and right middle temporal gyrus.

Nodal degree in the left supplementary motor area was only significantly decreased in PMS patients (108) compared to HC (112), but not in RRMS patients (115). Furthermore, both the nodal degree and path length in the left calcarine fissure (CAL.L), left dorsolateral cingulate gyrus (DCG.L), and right paracentral lobule (PCL.R) were only significantly affected in RRMS (CAL.L: 115; 1.36, DCG.L: 115; 1.45, PCL.R: 115; 1.55, respectively) but not in PMS patients (CAL.L: 115; 1.69, DCG.L: 113; 2.10, PCL.R: 110; 2.40, respectively) compared to HC (CAL.L: 112; 2.53, DCG.L: 110; 2.57, PCL.R: 105; 2.96, respectively). The nodal degree of the right putamen was only affected in RRMS patients (115) compared to HC (97), and not in PMS patients (100).

4.5. Discussion

MS is a very heterogeneous disease with pathogenesis and symptomatology varying per individual. However, similarities among symptoms and disability are found, suggesting the presence of a common pathway in the pathogenesis. Therefore, this study aimed to find regions that are affected in MS, which might indicate the region's importance in MS pathogenesis. In addition, we investigated whether regions are differentially affected between MS phenotypes and, most importantly, what the effect of lesion filling is on the calculation of graph theoretical network parameters derived from structural T_1w MRI images. Although lesion-filling introduced substantial artefacts for some lesions, it has significantly reduced the heterogeneity between MS patients, enabling detection of more differences in network parameters in a relatively small dataset. In general, the difference in global network parameters between the RRMS and HC group was larger than between the PMS and HC group, but no significant differences between the RRMS and PMS group were observed. Both in PMS and RRMS,

all investigated network parameters were affected on nodular level in the right Heschl gyrus, cerebellum crus 2, and cerebellum part 7b. This indicates the importance of these regions in MS pathogenesis.

Graph theoretical network analysis on original T_1w MRI data detected only a few differences between groups on a global level. The only global effects observed were a reduced modularity and a higher assortativity in MS patients, when compared to HC. Nodes with a high degree tend to be connected to nodes with a low degree, which results in a low assortativity.[427,436] The increased assortativity in MS patients therefore suggests a more random network, which is supported by the decreased modularity. On nodal level, a decrease in degree of the precentral gyrus is observed and an increase in degree of the left cerebellum part 6 and vermis part 6. As a higher degree indicates that the node is better connected, this seems contradictory to other literature that found that cerebellar dysfunction is common in MS.[437] However, functional reorganization to maintain high efficiency is a common phenomenon, which could lead to the generation of more connections in specific brain regions. The absence of significant differences for other network parameters in this study is likely due to the heterogeneity among MS patients, which can be caused by the random distribution of MS lesions or diffuse brain pathology. This implies that pathogenic effects are only observed when they are severe enough.

To compensate for the heterogeneity among MS patients and enhancing data-analysis sensitivity, lesion filling is often performed. Studies indicated that applying such a method enhances the reproducibility and reliability of GM and WM volume estimates.[438–440] This led to application of lesion filling for T_1w structural graph theoretical network analysis in several studies. Due to the dark intensity of MS lesions on T_1w MRI, however, lesion intensities can be similar to GM and therefore result in erroneous tissue segmentations. Since pathological changes represented by the lesions are omitted and a thorough evaluation of the effect of lesion filling has not yet been performed, the interpretability of the network analysis results after lesion-filling remains a matter of debate. Especially in graph theoretical network analysis, small changes in node intensity can have a substantial impact. For instance, if an affected hub is near a juxtacortical lesion, lesion filling might falsely insert extra GM voxels when “restoring” the structure, which might lead to erroneous results (see Fig. 4.3 & 4.4). In the current study, we also found a large number of artefacts arising from inaccurate lesion filling, especially in patients with a high number of lesions in the brain. The effects of minor artefacts, however, should be minimal, as they are considered to have no or negligible effects on tissue segmentation, and hence should hardly affect the calculation of the network parameters, if at all. However, for the substantial artefacts, the tissue segmentation is affected to some extent, but the effect on calculation of the network parameters might

be limited as the lesions occur at random locations and as such the artefacts caused by lesion filling as well. The artefacts would therefore only cause false negative results, and thus result in less significant findings. Therefore, studies applying lesion filling should carefully assess the lesion-filled images for artefacts, especially for datasets containing a high number of brain lesions. A possible solution to optimize the accuracy of lesion-filling could be to include only WM voxels for lesion-filling of juxtacortical WM lesions.

Despite the imperfection of the lesion filling method, the 95% CIs of the network parameters derived from the lesion-filled T_1w-based data were smaller than those derived from the original T_1w-based data. Consequently, a considerable increase in discriminative power was obtained when lesion filling was applied. The heterogeneity in MS results in a high variation in the number of lesions, the size of lesions, and the location of lesions between patients. The applied graph theoretical method calculates the network parameters group-wise, so it is expected that a high degree of heterogeneity among subjects would affect the robustness of these calculations. This might also explain the large increase in the number of significant findings when lesion filling was applied, and thus enables detection of subtle differences with small datasets.

Among the network parameters derived from the original T_1w MRI, differences were primarily detected on a global level. However, the original T_1w MRI dataset generated multiple nodular parameters that were significantly different between groups (uncorrected) in several affected regions, but these effects did not survive FDR correction. In contrast, lesion filled T_1w-based parameters showed significant differences on both a global and nodal level. This suggests that the results from lesion-filled MRI are not the result of the artefact introduced by the lesion filling method, since the differences are already present in the original data. Therefore, it seems likely that the variance in the original dataset was too high to reach statistical significance. By reducing the variance, lesion filling increases the statistical power. So, an alternative way to overcome the group heterogeneity could be using large sample sizes without lesion filling.

Using the lesion-filled T_1w dataset we found an increase in global and local efficiency and a decrease in modularity in MS patients, as compared to HC. This is in agreement with findings of Fleischer (2017), and Kocevar (2016),[425,427] and might suggest functional reorganization to maintain high cerebral efficiency. However, our findings of an increase in global and local efficiency and a decrease in modularity are in contrast to the results of other studies that found a decrease in global and local efficiency (He 2009, Shu 2011, Shu 2016, and Llufriu 2017).[421–423,428] Our study set-up is most similar to that of Kocevar, assessing different MS types with T_1w MRI, whereas He and co-workers did not use healthy controls and investigated only RRMS with T_1w MRI. The studies by Shu (2011),

Shu (2016), and Llufriu used DTI to investigate RRMS, CIS, and the total MS population, respectively. The discrepancy between these studies illustrate the difficulties of comparing the graph theoretical network parameters derived from different structural networks, like WM connectivity assessed with DTI, and GM connectivity assessed with T_1w.

Furthermore, our study shows that network parameters of RRMS patients in general deviate more from HC than those of PMS patients. This observation seems to be in agreement with the studies of Schoonheim and colleagues.[441–443] According to their hypothesis, functional reorganisation of the cerebral network takes place in MS patients as compensatory mechanism for structural damage, which is in agreement with our finding that a higher efficiency is found in RRMS patients than in HC. As a consequence, the network efficiency remains high enough for maintaining cognitive performances. However, there is a threshold for the functional reorganization capacity of the brain. When this threshold is reached, the brain is not able to fully compensate for the structural damage anymore, as suggested by the decreased efficiency observed in PMS compared to RRMS patients in this study. This is also supported by studies assessing axonal density in lesions that found a lower number of axons in progressive forms of MS compared to RRMS.[410,411,444] Thus, our results are in line with the findings of Fleischer, and Kocevar, and are supporting the Schoonheim hypothesis.[425,427,441]

Future studies should thoroughly evaluate the accuracy of current lesion filling methods and evaluate the generation of artefacts on both T_1w and tissue segmentations. Such a study would be able to determine the most optimal lesion filling method and indicate whether there is a need for further development of lesion filling methods. Until such a study is performed, no firm conclusions can be drawn regarding the optimal application of lesion filling. Nonetheless, our study clearly illustrates the positive effects lesion filling can have on the calculation of network parameters, despite the considerable number of artefacts generated, highlighting the need for cautious considerations before applying lesion filling.In conclusion, we found that the application of lesion filling has reduced the variability and increased the sensitivity of the structural T_1w network analysis. Although lesion filling is not perfect, we assume that application of lesion filling is especially important for studies with smaller sample sizes. In this study with a relatively small sample size, lesion filling indeed enabled graph theoretical network analysis to demonstrate that networks associated with cerebellum crus 2, cerebellum part 7b, and Heschl's gyrus are affected in all types of MS patients, and that networks involving the supplementary motor area are only significantly affected in PMS patients.

Acknowledgments

This study was supported by general electric (GE) Healthcare, grant number 12496139131 and the Nederlandse organisatie voor gezondheidsonderzoek en zorginnovatie (ZonMW) with Stichting MS research, grant number PTO-95105010.

Data availability statement

Due to privacy regulations the clinical data collected in this study are not deposited in a public registry, but the data can be made available via a request to the corresponding author.

Competing interests

The authors declare no competing interests related to this study.

Authors' contributions

CWJ, YH, and GDK analysed and interpreted the data, MP, KC, CR, CB, and DPF acquired and interpreted the data, CWJ, EFJ, JFM, MP, and DPF designed the study. All authors contributed to the interpretation of the data, writing and reviewing of the final manuscript.

4.6. Appendix

Appendix table 4.1: *Degree calculated from original T_1w*

HC vs. PMS								
	ROI	difference	p (2-tailed)	fdr (2-tailed)	HC	PMS	CI lower	CI upper
Frontal lobe								
	PreCG.L	-4	0.001	0.001	115	111	-1.00	1.00
	PreCG.R	-5	0.001	0.001	115	110	-2.00	2.00
Posterior fossa								
	C6.L	6	0.001	0.001	108	114	-3.01	2.99
	V6	14	0.001	0.001	101	115	-4.01	3.99

**solely the results of significantly different results that sustained FDR correction are presented*

Appendix table 4.2: *Degree calculated from lesion filled T_1w*

HC vs. MS total								
	ROI	difference	p (2-tailed)	fdr (2-tailed)	HC	MS total	CI lower	CI upper
Frontal								
	PreCG.L	1	0.010	0.030	114	115	0.00	0.00
	PreCG.R	1	0.006	0.030	114	115	0.00	0.00
	SFGdor.L	2	0.005	0.030	113	115	0.00	1.00
	SFGdor.R	3	0.001	0.030	112	115	0.00	1.00
	ORBsup.L	12	0.004	0.030	103	115	0.02	2.00
	MFG.R	2	0.003	0.030	113	115	0.00	1.00
	ORBmid.L	4	0.004	0.030	111	115	0.00	1.00
	ORBmid.R	6	0.002	0.030	109	115	0.00	1.00
	IFGtriang.R	3	0.007	0.030	112	115	0.00	1.00
	ORBinf.L	2	0.006	0.030	113	115	0.00	1.00
	ORBinf.R	1	0.026	0.030	114	115	0.00	1.00
	ROL.R	11	0.001	0.030	104	115	0.01	2.00
	SMA.L	3	0.018	0.030	112	115	0.00	2.00
	SMA.R	2	0.024	0.030	113	115	0.01	0.99
	OLF.R	3	0.029	0.030	112	115	0.01	1.99
	ORBsupmed.L	3	0.006	0.030	112	115	0.00	1.00
	ORBsupmed.R	6	0.008	0.030	109	115	0.01	1.99
	REC.L	4	0.018	0.030	111	115	0.00	1.99
	PCL.R	10	0.001	0.030	105	115	0.00	2.99
Insula and cingulate gyri								
	INS.R	3	0.008	0.030	112	115	0.00	2.00
	DCG.L	5	0.005	0.030	110	115	0.00	2.00
	DCG.R	4	0.001	0.030	111	115	0.00	1.00
	PCG.L	7	0.016	0.030	108	115	0.02	4.01
Temporal								
	AMYG.L	2	0.017	0.030	113	115	0.00	2.00
	AMYG.R	8	0.017	0.030	107	115	-0.01	4.99
	FFG.L	1	0.027	0.030	114	115	0.00	1.00
	FFG.R	5	0.006	0.030	110	115	0.01	1.00
	HES.L	2	0.008	0.030	113	115	0.00	1.00
	HES.R	7	0.001	0.030	108	115	0.01	0.99
	STG.L	3	0.003	0.030	112	115	0.00	1.00
	STG.R	1	0.010	0.030	114	115	0.00	1.00
	TPOsup.R	3	0.005	0.030	112	115	0.00	1.00
	MTG.L	6	0.001	0.030	109	115	0.00	0.00
	MTG.R	2	0.006	0.030	113	115	0.00	1.00
	TPOmid.R	3	0.030	0.030	112	115	-0.01	2.99
	ITG.L	8	0.002	0.030	107	115	0.01	0.99
	ITG.R	2	0.003	0.030	113	115	0.00	1.00

Occipital								
	CAL.L	3	0.007	0.030	112	115	0.00	1.00
	CUN.L	10	0.001	0.030	105	115	0.00	2.00
	LING.L	0	0.023	0.030	115	115	0.00	0.00
	LING.R	0	0.027	0.030	115	115	0.00	0.00
	SOG.R	8	0.001	0.030	107	115	0.00	1.00
	MOG.L	3	0.013	0.030	112	115	0.02	1.01
	MOG.R	3	0.028	0.030	112	115	0.01	2.00
	IOG.R	29	0.001	0.030	86	115	0.02	5.00
Parietal								
	SPG.L	3	0.017	0.030	112	115	0.01	1.99
	SPG.R	8	0.005	0.030	107	115	0.01	3.00
	IPL.L	1	0.018	0.030	114	115	0.00	1.00
	IPL.R	6	0.004	0.030	109	115	0.01	2.00
	SMG.L	2	0.006	0.030	113	115	0.00	1.00
	ANG.L	5	0.003	0.030	110	115	0.01	1.00
	ANG.R	1	0.028	0.030	114	115	0.00	1.00
	PCUN.L	8	0.001	0.030	107	115	0.00	2.00
	PCUN.R	5	0.002	0.030	110	115	0.00	2.00
Central								
	PUT.L	19	0.013	0.030	96	115	0.01	9.01
	THA.L	6	0.008	0.030	109	115	0.01	3.00
	THA.R	11	0.007	0.030	104	115	-0.01	3.49
Posterior fossa								
	CC1.R	13	0.001	0.030	102	115	0.01	3.00
	CC2.L	19	0.001	0.030	96	115	0.00	2.00
	CC2.R	32	0.001	0.030	83	115	0.00	4.01
	C3.L	4	0.010	0.030	111	115	0.01	2.00
	C3.R	5	0.015	0.030	110	115	-0.01	4.00
	C45.L	8	0.004	0.030	107	115	0.00	2.99
	C45.R	29	0.001	0.030	86	115	0.00	2.99
	C6.L	10	0.001	0.030	105	115	0.00	3.00
	C6.R	16	0.001	0.030	99	115	0.01	3.50
	C7b.R	28	0.001	0.030	87	115	0.01	2.99
	C8.L	2	0.008	0.030	113	115	0.00	1.00
	C8.R	3	0.003	0.030	112	115	0.00	1.00
	C9.L	4	0.021	0.030	111	115	0.00	3.00
	C9.R	6	0.002	0.030	109	115	0.00	2.00
	V6	6	0.020	0.030	109	115	-0.01	3.99
	V8	18	0.014	0.030	97	115	-1.03	9.98
	V9	14	0.019	0.030	101	115	0.03	7.02
HC vs. RRMS								

	ROI	difference	p (2-tailed)	fdr (2-tailed)	HC	RRMS	CI lower	CI upper
Frontal								
	PreCG.L	1	0.016	0.021	114	115	0.00	1.00
	PreCG.R	1	0.009	0.021	114	115	0.00	0.00
	SFGdor.L	2	0.002	0.021	113	115	0.00	0.00
	SFGdor.R	3	0.001	0.021	112	115	0.00	0.00
	ORBsup.L	12	0.009	0.021	103	115	0.00	3.99
	MFG.R	2	0.005	0.021	113	115	0.00	1.00
	ORBmid.L	4	0.020	0.021	111	115	-0.01	2.01
	ORBmid.R	6	0.007	0.021	109	115	-0.01	1.02
	ORBinf.L	2	0.005	0.021	113	115	-0.01	1.00
	ORBinf.R	1	0.021	0.021	114	115	0.00	0.99
	ROL.R	11	0.007	0.021	104	115	0.01	2.50
	SFGmed.R	1	0.014	0.021	114	115	0.00	0.00
	ORBsupmed.L	3	0.002	0.021	112	115	0.00	1.00
	PCL.R	10	0.008	0.021	105	115	-1.03	2.98
Insula and cingulate gyri								
	DCG.L	5	0.006	0.021	110	115	-0.01	1.00
	DCG.R	4	0.001	0.021	111	115	0.00	1.00
Occipital								
	CAL.L	3	0.017	0.021	112	115	0.00	2.00
	CUN.L	10	0.003	0.021	105	115	-0.01	1.99
	LING.L	0	0.008	0.021	115	115	0.00	0.00
	LING.R	0	0.016	0.021	115	115	0.00	0.00
	SOG.R	8	0.002	0.021	107	115	-0.01	2.00
	MOG.L	3	0.013	0.021	112	115	0.00	1.00
	IOG.R	29	0.001	0.021	86	115	-0.99	7.00
Parietal								
	SPG.R	8	0.017	0.021	107	115	-1.01	5.00
	IPL.L	1	0.013	0.021	114	115	0.00	1.00
	IPL.R	6	0.012	0.021	109	115	-0.01	2.99
	SMG.L	2	0.006	0.021	113	115	0.00	1.00
	ANG.L	5	0.002	0.021	110	115	0.01	1.00
	PCUN.L	8	0.009	0.021	107	115	-0.02	2.98
	PCUN.R	5	0.011	0.021	110	115	-0.01	1.99
Central								
	PUT.L	19	0.001	0.021	96	115	-0.02	4.02
	PUT.R	18	0.017	0.021	97	115	-0.99	9.99
	THA.L	6	0.005	0.021	109	115	0.00	1.99
	THA.R	11	0.001	0.021	104	115	-1.00	3.00
Temporal								
	HES.L	2	0.012	0.021	113	115	0.00	1.00
	HES.R	7	0.002	0.021	108	115	-0.01	1.00
	STG.L	3	0.011	0.021	112	115	0.00	1.00

	STG.R	1	0.013	0.021	114	115	0.01	0.01
	TPOsup.R	3	0.011	0.021	112	115	0.00	2.00
	MTG.L	6	0.001	0.021	109	115	0.00	0.00
	MTG.R	2	0.010	0.021	113	115	0.01	1.00
	ITG.L	8	0.010	0.021	107	115	-0.01	1.00
	ITG.R	2	0.012	0.021	113	115	0.00	1.00
Posterior fossa								
	CC1.R	13	0.005	0.021	102	115	-1.00	3.99
	CC2.L	19	0.001	0.021	96	115	-0.99	3.00
	CC2.R	32	0.001	0.021	83	115	-1.01	4.00
	C45.L	8	0.010	0.021	107	115	-0.99	3.50
	C45.R	29	0.001	0.021	86	115	-2.00	4.98
	C6.L	10	0.002	0.021	105	115	-1.00	3.01
	C6.R	16	0.004	0.021	99	115	-0.99	4.00
	C7b.L	1	0.016	0.021	114	115	0.00	1.00
	C7b.R	28	0.001	0.021	87	115	-1.01	3.99
	C8.L	2	0.018	0.021	113	115	-0.01	0.99
	C8.R	3	0.007	0.021	112	115	0.00	0.99
	C9.R	6	0.017	0.021	109	115	-1.00	4.00
	V7	5	0.019	0.021	110	115	-0.01	2.99
	V8	18	0.020	0.021	97	115	-3.03	10.03
	V9	14	0.011	0.021	101	115	-1.01	5.00
HC vs. PMS								
	ROI	difference	p (2-tailed)	fdr (2-tailed)	HC	PMS	CI lower	CI upper
Frontal								
	PreCG.L	1	0.006	0.024	114	115	0.00	0.00
	PreCG.R	1	0.007	0.024	114	115	0.00	0.00
	SFGdor.L	2	0.007	0.024	113	115	-1.00	1.00
	SFGdor.R	3	0.001	0.024	112	115	-1.00	1.00
	ORBsup.L	12	0.001	0.024	103	115	-2.00	1.01
	MFG.R	2	0.008	0.024	113	115	-1.00	1.00
	ORBmid.L	4	0.006	0.024	111	115	-1.00	1.00
	ORBmid.R	6	0.005	0.024	109	115	-2.01	1.99
	IFGtriang.R	3	0.007	0.024	112	115	-1.00	1.00
	ORBinf.L	2	0.007	0.024	113	115	-1.00	1.00
	ROL.R	11	0.001	0.024	104	115	-2.00	1.00
	SMA.L	-4	0.005	0.024	112	108	-1.01	1.00
	OLF.R	3	0.007	0.024	112	115	-1.01	1.01
	SFGmed.R	1	0.024	0.024	114	115	-1.00	1.00
	ORBsupmed.L	3	0.003	0.024	112	115	-1.01	1.00
	ORBsupmed.R	6	0.003	0.024	109	115	-1.01	1.01
	REC.L	4	0.010	0.024	111	115	-1.01	0.99

Insula and cingulate gyri								
	DCG.R	3	0.007	0.024	111	114	-1.01	1.00
Temporal								
	AMYG.L	2	0.024	0.024	113	115	-1.00	1.00
	AMYG.R	8	0.016	0.024	107	115	-4.00	3.99
	FFG.R	5	0.009	0.024	110	115	-1.00	1.00
	HES.L	2	0.008	0.024	113	115	-1.00	0.00
	HES.R	7	0.001	0.024	108	115	0.00	0.00
	STG.L	3	0.001	0.024	112	115	0.00	0.00
	STG.R	1	0.016	0.024	114	115	-1.01	-0.01
	TPOsup.R	3	0.005	0.024	112	115	-1.00	1.00
	MTG.L	6	0.001	0.024	109	115	-1.00	0.00
	MTG.R	2	0.024	0.024	113	115	-1.00	1.00
	TPOmid.L	3	0.017	0.024	112	115	-2.00	2.00
	TPOmid.R	3	0.018	0.024	112	115	-2.01	2.00
	ITG.L	8	0.001	0.024	107	115	0.00	0.00
	ITG.R	2	0.015	0.024	113	115	-1.00	1.00
Occipital								
	CAL.R	-3	0.023	0.024	115	112	-1.00	1.00
	CUN.L	10	0.001	0.024	105	115	-2.00	1.99
	LING.L	0	0.012	0.024	115	115	0.00	0.00
	LING.R	0	0.024	0.024	115	115	0.00	0.00
	SOG.R	8	0.001	0.024	107	115	-2.50	2.00
	MOG.L	3	0.004	0.024	112	115	-1.00	0.00
	IOG.R	29	0.015	0.024	86	115	-10.99	8.97
Parietal								
	SPG.R	7	0.008	0.024	107	114	-4.00	4.01
	IPL.R	5	0.012	0.024	109	114	-2.50	1.99
	SMG.L	2	0.012	0.024	113	115	-0.01	-0.01
	ANG.L	5	0.004	0.024	110	115	-1.01	0.99
	ANG.R	1	0.023	0.024	114	115	-1.00	0.00
	PCUN.L	7	0.003	0.024	107	114	-2.99	2.99
	PCUN.R	4	0.003	0.024	110	114	-2.00	2.00
Central								
	THA.L	6	0.024	0.024	109	115	-1.99	1.98
	THA.R	11	0.019	0.024	104	115	-3.00	3.50
Posterior fossa								
	CC1.R	13	0.001	0.024	102	115	-3.99	3.01
	CC2.L	18	0.001	0.024	96	114	-4.00	4.00
	CC2.R	28	0.003	0.024	83	111	-6.99	7.03
	C3.L	4	0.003	0.024	111	115	-1.00	1.00
	C3.R	5	0.009	0.024	110	115	-3.01	2.00
	C45.L	8	0.002	0.024	107	115	-1.00	1.01
	C45.R	28	0.001	0.024	86	114	-3.02	3.01
	C6.L	10	0.003	0.024	105	115	-3.02	2.99

	C6.R	16	0.001	0.024	99	115	-5.01	5.00
	C7b.R	28	0.001	0.024	87	115	-5.00	2.98
	C8.L	2	0.005	0.024	113	115	-1.00	1.00
	C8.R	3	0.006	0.024	112	115	-2.00	1.00
	C9.L	4	0.007	0.024	111	115	-1.00	1.00
	C9.R	6	0.003	0.024	109	115	-2.01	1.00

**solely the results of significantly different results that sustained FDR correction are presented*

Appendix table 4.3: *Strength calculated from lesion filled T_1w*

HC vs. MS total								
	ROI	difference	p (2-tailed)	fdr (2-tailed)	HC	MS total	CI lower	CI upper
Frontal								
	MFG.R	29.0	0.014	0.014	55.0	83.9	-14.1	19.3
	ORBmid.L	31.7	0.009	0.014	48.8	80.5	-16.7	22.3
	ORBmid.R	39.9	0.002	0.014	42.2	82.1	-15.5	22.9
	IFGtriang.R	30.9	0.006	0.014	50.6	81.6	-15.1	21.4
	ORBinf.L	31.5	0.005	0.014	54.6	86.1	-13.8	21.3
	ORBinf.R	25.2	0.012	0.014	59.4	84.6	-12.3	19.7
	ROL.R	41.7	0.005	0.014	36.8	78.5	-18.5	25.1
	PCL.R	38.1	0.013	0.014	31.0	69.1	-21.8	27.6
Insula and cingulate gyri								
	DCG.R	33.5	0.008	0.014	46.6	80.1	-15.3	23.1
Temporal								
	AMYG.L	40.4	0.002	0.014	35.7	76.0	-16.5	22.3
	HES.R	39.0	0.001	0.014	40.3	79.4	-13.2	20.2
	STG.L	27.8	0.014	0.014	51.6	79.4	-15.2	21.2
	STG.R	31.7	0.002	0.014	54.8	86.5	-11.5	18.0
	TPOsup.L	25.3	0.011	0.014	54.4	79.7	-11.0	18.8
	TPOsup.R	27.1	0.011	0.014	52.6	79.7	-12.0	19.6
	MTG.L	33.4	0.002	0.014	51.2	84.6	-12.1	18.8
	MTG.R	31.7	0.005	0.014	54.4	86.2	-13.0	19.8
	ITG.R	36.3	0.002	0.014	49.0	85.4	-13.6	21.0
Occipital								
	CAL.L	39.3	0.003	0.014	44.6	83.9	-15.9	23.2
	CUN.L	47.3	0.001	0.014	37.6	84.9	-16.5	26.4
	SOG.R	43.0	0.003	0.014	35.4	78.4	-17.9	24.6
Parietal								
	PoCG.R	31.8	0.002	0.014	53.2	85.0	-12.2	19.0
	SPG.R	42.5	0.008	0.014	33.3	75.8	-21.5	29.5
	IPL.R	36.9	0.010	0.014	39.7	76.5	-18.8	25.4
	PCUN.L	42.0	0.004	0.014	37.3	79.3	-19.8	27.8
	PCUN.R	41.6	0.003	0.014	39.6	81.3	-17.4	24.3
Posterior fossa								
	CC1.L	33.0	0.004	0.014	47.2	80.2	-13.1	20.7
	CC1.R	53.7	0.001	0.014	25.0	78.7	-18.5	27.4
	CC2.L	52.2	0.001	0.014	27.6	79.8	-15.5	22.9
	CC2.R	55.4	0.001	0.014	18.9	74.3	-21.0	30.4
	C45.R	46.5	0.003	0.014	25.3	71.8	-18.9	26.8
	C6.L	38.9	0.006	0.014	38.9	77.8	-17.1	25.3
	C6.R	45.0	0.001	0.014	33.7	78.7	-17.5	27.6
	C7b.L	31.1	0.003	0.014	46.7	77.8	-14.6	20.9

	C7b.R	55.9	0.001	0.014	19.5	75.4	-18.8	26.0
	C8.L	33.5	0.007	0.014	42.4	75.9	-16.1	23.0
	C8.R	36.2	0.004	0.014	41.0	77.1	-16.0	22.6
HC vs. RRMS								
	ROI	difference	p (2-tailed)	fdr (2-tailed)	HC	RRMS	CI lower	CI upper
Frontal								
	ORBmid.R	42.5	0.002	0.002	42.2	84.7	-23.2	26.9
Temporal								
	HES.R	39.5	0.001	0.002	40.3	79.9	-19.6	24.8
Posterior fossa								
	CC2.L	55.1	0.001	0.002	27.6	82.7	-22.2	26.0
	CC2.R	61.6	0.001	0.002	18.9	80.5	-25.4	30.2
	C7b.R	60.7	0.001	0.002	19.5	80.3	-26.4	30.6

**solely the results of significantly different results that sustained FDR correction are presented*

Appendix table 4.4: *Path length calculated from lesion filled T_1w*

HC vs. MS total								
	ROI	difference	p (2-tailed)	fdr (2-tailed)	HC	MS total	CI lower	CI upper
Frontal								
	PreCG.L	-0.67	0.009	0.024	2.12	1.45	-0.48	0.24
	PreCG.R	-0.71	0.007	0.024	2.16	1.45	-0.43	0.23
	SFGdor.L	-0.74	0.007	0.024	2.21	1.47	-0.45	0.23
	SFGdor.R	-0.80	0.011	0.024	2.27	1.47	-0.48	0.26
	ORBsup.R	-0.97	0.012	0.024	2.49	1.52	-0.70	0.38
	MFG.R	-0.79	0.005	0.024	2.21	1.42	-0.46	0.23
	ORBmid.L	-0.87	0.006	0.024	2.37	1.50	-0.58	0.32
	ORBmid.R	-1.09	0.001	0.024	2.55	1.46	-0.56	0.31
	IFGoperc.R	-0.77	0.013	0.024	2.29	1.52	-0.51	0.27
	IFGtriang.L	-0.59	0.021	0.024	2.06	1.47	-0.45	0.27
	IFGtriang.R	-0.85	0.005	0.024	2.32	1.47	-0.54	0.30
	ORBinf.L	-0.81	0.002	0.024	2.19	1.38	-0.48	0.26
	ORBinf.R	-0.65	0.006	0.024	2.07	1.42	-0.42	0.23
	ROL.L	-0.61	0.022	0.024	2.06	1.45	-0.50	0.27
	ROL.R	-1.20	0.001	0.024	2.74	1.54	-0.64	0.38
	SFGmed.L	-0.57	0.023	0.024	2.07	1.50	-0.43	0.24
	ORBsupmed.L	-0.64	0.023	0.024	2.16	1.52	-0.51	0.28
	PCL.R	-1.22	0.004	0.024	2.96	1.74	-0.81	0.50
Insula and cingulate gyri								
	INS.R	-0.85	0.012	0.024	2.37	1.52	-0.65	0.34
	ACG.L	-0.76	0.018	0.024	2.35	1.59	-0.57	0.33
	DCG.L	-0.95	0.023	0.024	2.57	1.62	-0.76	0.42
	DCG.R	-1.03	0.005	0.024	2.51	1.48	-0.55	0.29
	PCG.L	-1.31	0.019	0.024	3.03	1.71	-0.97	0.67
Temporal								
	HIP.L	-0.71	0.024	0.024	2.43	1.72	-0.60	0.37
	AMYG.L	-1.40	0.001	0.024	2.96	1.55	-0.62	0.35
	HES.L	-0.74	0.013	0.024	2.23	1.49	-0.52	0.27
	HES.R	-1.16	0.001	0.024	2.65	1.49	-0.51	0.25
	STG.L	-0.79	0.008	0.024	2.29	1.50	-0.51	0.28
	STG.R	-0.81	0.001	0.024	2.19	1.38	-0.38	0.20
	TPOsup.L	-0.67	0.005	0.024	2.18	1.51	-0.39	0.22
	TPOsup.R	-0.73	0.005	0.024	2.24	1.50	-0.45	0.24
	MTG.L	-0.86	0.001	0.024	2.27	1.40	-0.40	0.21
	MTG.R	-0.84	0.001	0.024	2.22	1.38	-0.46	0.24
	TPOmid.R	-0.96	0.021	0.024	2.64	1.69	-0.75	0.47
	ITG.L	-0.87	0.013	0.024	2.36	1.49	-0.64	0.35
	ITG.R	-0.98	0.001	0.024	2.37	1.40	-0.47	0.25
Occipital								
	CAL.L	-1.11	0.001	0.024	2.53	1.42	-0.54	0.29

	CUN.L	-1.36	0.001	0.024	2.75	1.39	-0.57	0.34
	LING.L	-0.60	0.019	0.024	2.05	1.45	-0.45	0.24
	LING.R	-0.61	0.023	0.024	2.04	1.44	-0.46	0.24
	SOG.R	-1.40	0.001	0.024	2.91	1.51	-0.67	0.38
	IOG.R	-1.50	0.008	0.024	3.14	1.64	-1.03	0.73
Parietal								
	PoCG.L	-0.61	0.009	0.024	2.06	1.45	-0.39	0.21
	PoCG.R	-0.86	0.001	0.024	2.26	1.40	-0.40	0.21
	SPG.R	-1.36	0.004	0.024	2.95	1.58	-0.82	0.51
	IPL.L	-0.69	0.013	0.024	2.16	1.47	-0.46	0.25
	IPL.R	-1.10	0.012	0.024	2.68	1.58	-0.69	0.40
	SMG.L	-0.82	0.009	0.024	2.29	1.46	-0.54	0.28
	SMG.R	-0.80	0.011	0.024	2.23	1.43	-0.54	0.29
	ANG.R	-0.72	0.016	0.024	2.18	1.46	-0.52	0.27
	PCUN.L	-1.27	0.004	0.024	2.77	1.50	-0.71	0.38
	PCUN.R	-1.21	0.002	0.024	2.67	1.46	-0.60	0.32
Posterior fossa								
	CC1.L	-0.92	0.003	0.024	2.40	1.48	-0.51	0.26
	CC1.R	-1.78	0.001	0.024	3.29	1.51	-0.73	0.40
	CC2.L	-1.65	0.001	0.024	3.15	1.50	-0.56	0.31
	CC2.R	-2.10	0.001	0.024	3.72	1.62	-0.85	0.49
	C3.R	-1.01	0.012	0.024	2.74	1.73	-0.74	0.45
	C45.L	-0.99	0.007	0.024	2.75	1.76	-0.71	0.42
	C45.R	-1.62	0.001	0.024	3.28	1.66	-0.72	0.43
	C6.L	-1.24	0.002	0.024	2.77	1.53	-0.61	0.36
	C6.R	-1.37	0.001	0.024	2.88	1.51	-0.68	0.38
	C7b.L	-0.94	0.002	0.024	2.48	1.53	-0.50	0.27
	C7b.R	-2.06	0.001	0.024	3.66	1.59	-0.72	0.40
	C8.L	-1.05	0.005	0.024	2.60	1.55	-0.61	0.33
	C8.R	-1.07	0.002	0.024	2.61	1.54	-0.56	0.32
	C9.L	-0.96	0.023	0.024	2.83	1.87	-0.78	0.49
	C9.R	-1.05	0.007	0.024	2.77	1.72	-0.74	0.43
HC vs. RRMS								
	ROI	difference	p (2-tailed)	fdr (2-tailed)	HC	RRMS	CI lower	CI upper
Frontal								
	ORBmid.R	-1.15	0.005	0.009	2.55	1.40	-0.69	0.53
	ROL.R	-1.29	0.005	0.009	2.74	1.44	-0.84	0.64
	PCL.R	-1.41	0.004	0.009	2.96	1.55	-0.87	0.71
Insula and cingulate gyri								
	DCG.L	-1.13	0.006	0.009	2.57	1.45	-0.70	0.50
	DCG.R	-1.12	0.005	0.009	2.51	1.39	-0.67	0.48
Temporal								
	AMYG.L	-1.42	0.002	0.009	2.96	1.54	-0.79	0.63

	HES.R	-1.17	0.001	0.009	2.65	1.49	-0.62	0.46
	STG.R	-0.86	0.005	0.009	2.19	1.33	-0.52	0.38
	MTG.L	-0.93	0.003	0.009	2.27	1.34	-0.51	0.36
	MTG.R	-0.89	0.005	0.009	2.22	1.33	-0.57	0.38
	ITG.R	-1.02	0.004	0.009	2.37	1.35	-0.61	0.43
Occipital								
	CAL.L	-1.17	0.006	0.009	2.53	1.36	-0.71	0.53
	CUN.L	-1.38	0.005	0.009	2.75	1.37	-0.80	0.61
	SOG.R	-1.46	0.002	0.009	2.91	1.45	-0.79	0.60
	IOG.R	-1.56	0.006	0.009	3.14	1.58	-1.03	0.94
Parietal								
	PoCG.R	-0.88	0.008	0.009	2.26	1.39	-0.52	0.36
	PCUN.L	-1.27	0.009	0.009	2.77	1.50	-0.93	0.68
	PCUN.R	-1.23	0.009	0.009	2.67	1.44	-0.83	0.62
Posterior fossa								
	CC1.R	-1.75	0.001	0.009	3.29	1.54	-0.93	0.72
	CC2.L	-1.72	0.001	0.009	3.15	1.43	-0.71	0.54
	CC2.R	-2.25	0.001	0.009	3.72	1.47	-0.83	0.64
	C45.R	-1.72	0.001	0.009	3.28	1.55	-0.88	0.73
	C6.L	-1.27	0.004	0.009	2.77	1.50	-0.78	0.55
	C6.R	-1.44	0.003	0.009	2.88	1.44	-0.80	0.61
	C7b.R	-2.17	0.001	0.009	3.66	1.48	-0.87	0.68
	C8.R	-1.08	0.007	0.009	2.61	1.53	-0.78	0.52
HC vs. PMS								
	ROI	difference	p (2-tailed)	fdr (2-tailed)	HC	PMS	CI lower	CI upper
Occipital								
	CUN.L	-1.25	0.003	0.003	2.75	1.50	-0.67	0.63
Parietal								
	PoCG.R	-0.74	0.001	0.003	2.26	1.52	-0.34	0.33
Temporal								
	HES.R	-1.03	0.001	0.003	2.65	1.63	-0.46	0.44
	TPOsup.R	-0.69	0.001	0.003	2.24	1.55	-0.37	0.33
Posterior fossa								
	CC1.R	-1.60	0.001	0.003	3.29	1.69	-0.84	0.74
	CC2.L	-1.41	0.001	0.003	3.15	1.74	-0.70	0.63
	C7b.L	-0.84	0.001	0.003	2.48	1.63	-0.38	0.35
	C7b.R	-1.91	0.001	0.003	3.66	1.74	-0.86	0.82
	C8.R	-0.89	0.003	0.003	2.61	1.73	-0.49	0.47

**solely the results of significantly different results that sustained FDR correction are presented*

Appendix table 4.5: *Global efficiency calculated from lesion filled T_1w*

HC vs. MS total								
	ROI	difference	p (2-tailed)	fdr (2-tailed)	HC	MS total	CI lower	CI upper
Posterior fossa								
	CC1.R	0.36	0.001	0.001	0.32	0.68	-0.16	0.22
	CC2.L	0.36	0.001	0.001	0.34	0.69	-0.13	0.18
	C7b.R	0.37	0.001	0.001	0.29	0.66	-0.16	0.21
HC vs. RRMS								
	ROI	difference	p (2-tailed)	fdr (2-tailed)	HC	RRMS	CI lower	CI upper
Posterior fossa								
	CC2.L	0.38	0.001	0.001	0.34	0.72	-0.19	0.21
	CC2.R	0.42	0.001	0.001	0.28	0.70	-0.22	0.22
	C7b.R	0.41	0.001	0.001	0.29	0.70	-0.22	0.23

**solely the results of significantly different results that sustained FDR correction are presented*

Appendix table 4.6: *Clustering coefficient calculated from lesion filled T_1w*

HC vs. MS total								
	ROI	difference	p (2-tailed)	fdr (2-tailed)	HC	MS total	CI lower	CI upper
Frontal								
	PreCG.L	0.25	0.016	0.024	0.44	0.68	-0.12	0.19
	PreCG.R	0.25	0.016	0.024	0.43	0.68	-0.12	0.19
	SFGdor.L	0.26	0.011	0.024	0.42	0.68	-0.12	0.18
	SFGdor.R	0.26	0.013	0.024	0.41	0.68	-0.12	0.20
	ORBsup.R	0.30	0.011	0.024	0.36	0.66	-0.13	0.22
	MFG.R	0.27	0.010	0.024	0.42	0.69	-0.12	0.18
	ORBmid.L	0.29	0.007	0.024	0.39	0.67	-0.13	0.20
	ORBmid.R	0.33	0.002	0.024	0.35	0.68	-0.13	0.19
	IFGoperc.R	0.27	0.012	0.024	0.40	0.66	-0.12	0.19
	IFGtriang.L	0.24	0.014	0.024	0.43	0.68	-0.12	0.18
	IFGtriang.R	0.29	0.009	0.024	0.39	0.68	-0.12	0.19
	ORBinf.L	0.28	0.006	0.024	0.42	0.70	-0.11	0.19
	ORBinf.R	0.26	0.010	0.024	0.44	0.70	-0.10	0.18
	ROL.L	0.24	0.021	0.024	0.44	0.68	-0.12	0.19
	ROL.R	0.33	0.005	0.024	0.33	0.66	-0.14	0.21
	SFGmed.L	0.24	0.021	0.024	0.44	0.67	-0.11	0.19
	PCL.R	0.32	0.022	0.024	0.28	0.61	-0.16	0.25
Insula and cingulate gyri								
	INS.L	0.24	0.014	0.024	0.45	0.68	-0.11	0.18
	INS.R	0.28	0.006	0.024	0.38	0.67	-0.13	0.19
	ACG.L	0.26	0.016	0.024	0.39	0.64	-0.13	0.20
	DCG.R	0.29	0.009	0.024	0.38	0.67	-0.13	0.20
	PCG.L	0.31	0.020	0.024	0.30	0.61	-0.17	0.24
Temporal								
	AMYG.L	0.34	0.004	0.024	0.31	0.65	-0.13	0.19
	FFG.L	0.26	0.023	0.024	0.43	0.68	-0.12	0.20
	HES.L	0.26	0.015	0.024	0.41	0.67	-0.12	0.19
	HES.R	0.31	0.004	0.024	0.35	0.67	-0.11	0.18
	STG.L	0.26	0.010	0.024	0.40	0.67	-0.12	0.18
	STG.R	0.30	0.002	0.024	0.41	0.71	-0.10	0.17
	TPOsup.L	0.25	0.008	0.024	0.42	0.67	-0.11	0.17
	TPOsup.R	0.26	0.010	0.024	0.41	0.67	-0.11	0.18
	MTG.L	0.29	0.003	0.024	0.40	0.70	-0.10	0.17
	MTG.R	0.29	0.005	0.024	0.42	0.70	-0.11	0.18
	ITG.L	0.27	0.020	0.024	0.40	0.67	-0.14	0.21
	ITG.R	0.32	0.002	0.024	0.38	0.70	-0.11	0.19
Occipital								
	CAL.L	0.33	0.004	0.024	0.36	0.69	-0.13	0.20
	CUN.L	0.36	0.003	0.024	0.34	0.70	-0.14	0.22
	LING.L	0.24	0.024	0.024	0.44	0.68	-0.12	0.19

	SOG.R	0.34	0.002	0.024	0.32	0.66	-0.14	0.21
Parietal								
	PoCG.L	0.24	0.018	0.024	0.45	0.68	-0.11	0.18
	PoCG.R	0.30	0.002	0.024	0.40	0.70	-0.11	0.18
	SPG.R	0.35	0.009	0.024	0.29	0.65	-0.16	0.23
	IPL.L	0.25	0.013	0.024	0.42	0.68	-0.12	0.19
	IPL.R	0.31	0.012	0.024	0.34	0.65	-0.15	0.21
	SMG.L	0.27	0.011	0.024	0.41	0.68	-0.12	0.20
	SMG.R	0.29	0.009	0.024	0.40	0.69	-0.13	0.20
	ANG.R	0.26	0.022	0.024	0.43	0.68	-0.13	0.20
	PCUN.L	0.35	0.006	0.024	0.32	0.67	-0.15	0.22
	PCUN.R	0.34	0.004	0.024	0.33	0.68	-0.13	0.20
Posterior fossa								
	CC1.L	0.31	0.005	0.024	0.36	0.67	-0.12	0.19
	CC1.R	0.41	0.001	0.024	0.25	0.66	-0.15	0.21
	CC2.L	0.39	0.001	0.024	0.28	0.67	-0.12	0.19
	CC2.R	0.40	0.002	0.024	0.24	0.64	-0.15	0.23
	C3.R	0.29	0.017	0.024	0.32	0.61	-0.15	0.22
	C45.R	0.35	0.004	0.024	0.27	0.62	-0.14	0.21
	C6.L	0.32	0.004	0.024	0.33	0.66	-0.14	0.20
	C6.R	0.35	0.003	0.024	0.31	0.66	-0.15	0.21
	C7b.L	0.29	0.004	0.024	0.37	0.66	-0.11	0.18
	C7b.R	0.41	0.001	0.024	0.24	0.64	-0.13	0.21
	C8.L	0.31	0.004	0.024	0.34	0.65	-0.12	0.20
	C8.R	0.32	0.003	0.024	0.33	0.65	-0.12	0.20
	C9.R	0.28	0.018	0.024	0.32	0.60	-0.15	0.20
	C10.R	0.25	0.022	0.024	0.38	0.62	-0.13	0.21
HC vs. RRMS								
	ROI	difference	p (2-tailed)	fdr (2-tailed)	HC	RRMS	CI lower	CI upper
Posterior fossa								
	CC1.R	0.41	0.001	0.001	0.25	0.66	-0.21	0.26
	CC2.R	0.44	0.001	0.001	0.24	0.68	-0.21	0.24
	C7b.R	0.44	0.001	0.001	0.24	0.68	-0.20	0.24

**solely the results of significantly different results that sustained FDR correction are presented*

Appendix table 4.7: *AAL atlas ROI abbreviations and full names*

	AAL label	Abbreviation	Full name
Temporal lobe			
	37	HIP.L	Left Hippocampus
	38	HIP.R	Right Hippocampus
	39	PHG.L	Left Parahippocampal gyrus
	40	PHG.R	Right Parahippocampal gyrus
	41	AMYG.L	Left Amygdala
	42	AMYG.R	Right Amygdala
	55	FFG.L	Left Fusiform gyrus
	56	FFG.R	Right Fusiform gyrus
	79	HES.L	Left Heschl gyrus
	80	HES.R	Right Heschl gyrus
	81	STG.L	Left Superior temporal gyrus
	82	STG.R	Right Superior temporal gyrus
	83	TPOsup.L	Left Temporal pole: superior temporal gyrus
	84	TPOsup.R	Right Temporal pole: superior temporal gyrus
	85	MTG.L	Left Middle temporal gyrus
	86	MTG.R	Right Middle temporal gyrus
	87	TPOmid.L	Left Temporal pole: middle temporal gyrus
	88	TPOmid.R	Right Temporal pole: middle temporal gyrus
	89	ITG.L	Left Inferior temporal gyrus
	90	ITG.R	Right Inferior temporal gyrus
Frontal lobe			
	1	PreCG.L	Left Precental gyrus
	2	PreCG.R	Right Precental gyrus
	3	SFGdor.L	Left Superior frontal gyrus, dorsolateral
	4	SFGdor.R	Right Superior frontal gyrus, dorsolateral
	5	ORBsup.L	Left Superior frontal gyrus, orbital part
	6	ORBsup.R	Right Superior frontal gyrus, orbital part
	7	MFG.L	Left Middle frontal gyrus
	8	MFG.R	Right Middle frontal gyrus
	9	ORBmid.L	Left Middle frontal gyrus, orbital part
	10	ORBmid.R	Right Middle frontal gyrus, orbital part
	11	IFGoperc.L	Left Inferior frontal gyrus, opercular part
	12	IFGoperc.R	Right Inferior frontal gyrus, opercular part
	13	IFGtriang.L	Left Inferior frontal gyrus, triangular part
	14	IFGtriang.R	Right Inferior frontal gyrus, triangular part
	15	ORBinf.L	Left Inferior frontal gyrus, orbital part
	16	ORBinf.R	Right Inferior frontal gyrus, orbital part
	17	ROL.L	Left Rolandic operculum

	18	ROL.R	Right Rolandic operculum
	19	SMA.L	Left Supplementary motor area
	20	SMA.R	Right Supplementary motor area
	21	OLF.L	Left Olfactory cortex
	22	OLF.R	Right Olfactory cortex
	23	SFGmed.L	Left Superior frontal gyrus, medial
	24	SFGmed.R	Right Superior frontal gyrus, medial
	25	ORBsupmed.L	Left Superior frontal gyrus, medial orbital
	26	ORBsupmed.R	Right Superior frontal gyrus, medial orbital
	27	REC.L	Left Gyrus rectus
	28	REC.R	Right Gyrus rectus
	69	PCL.L	Left Paracentral lobule
	70	PCL.R	Right Paracentral lobule
Occipital lobe			
	43	CAL.L	Left Calcarine fissure and surrounding cortex
	44	CAL.R	Right Calcarine fissure and surrounding cortex
	45	CUN.L	Left Cuneus
	46	CUN.R	Right Cuneus
	47	LING.L	Left Lingual gyrus
	48	LING.R	Right Lingual gyrus
	49	SOG.L	Left Superior occipital gyrus
	50	SOG.R	Right Superior occipital gyrus
	51	MOG.L	Left Middle occipital gyrus
	52	MOG.R	Right Middle occipital gyrus
	53	IOG.L	Left Inferior occipital gyrus
	54	IOG.R	Right Inferior occipital gyrus
Parietal lobe			
	57	PoCG.L	Left Postcentral gyrus
	58	PoCG.R	Right Postcentral gyrus
	59	SPG.L	Left Superior parietal gyrus
	60	SPG.R	Right Superior parietal gyrus
	61	IPL.L	Left Inferior parietal, but supramarginal and angular gyri
	62	IPL.R	Right Inferior parietal, but supramarginal and angular gyri
	63	SMG.L	Left Supramarginal gyrus
	64	SMG.R	Right Supramarginal gyrus
	65	ANG.L	Left Angular gyrus
	66	ANG.R	Right Angular gyrus
	67	PCUN.L	Left Precuneus
	68	PCUN.R	Right Precuneus
Insula and Cingulate gyri			
	29	INS.L	Left Insula

	30	INS.R	Right Insula
	31	ACG.L	Left Anterior cingulate and paracingulate gyri
	32	ACG.R	Right Anterior cingulate and paracingulate gyri
	33	DCG.L	Left Median cingulate and paracingulate gyri
	34	DCG.R	Right Median cingulate and paracingulate gyri
	35	PCG.L	Left Posterior cingulate gyrus
	36	PCG.R	Right Posterior cingulate gyrus
Central structures			
	71	CAU.L	Left Caudate nucleus
	72	CAU.R	Right Caudate nucleus
	73	PUT.L	Left Lenticular nucleus, putamen
	74	PUT.R	Right Lenticular nucleus, putamen
	75	PAL.L	Left Lenticular nucleus, pallidum
	76	PAL.R	Right Lenticular nucleus, pallidum
	77	THA.L	Left Thalamus
	78	THA.R	Thalamus
Posterior fossa			
	91	CC1.L	Left Cerebellum crus part 1
	92	CC1.R	Right Cerebellum crus part 1
	93	CC2.L	Left Cerebellum crus part 2
	94	CC2.R	Right Cerebellum crus part 2
	95	C3.L	Left Cerebellum part 3
	96	C3.R	Right Cerebellum part 3
	97	C45.L	Left Cerebellum part 4 & 5
	98	C45.R	Right Cerebellum part 4 & 5
	99	C6.L	Left Cerebellum part 6
	100	C6.R	Right Cerebellum part 6
	101	C7b.L	Left Cerebellum part 7b
	102	C7b.R	Right Cerebellum part 7b
	103	C8.L	Left Cerebellum part 8
	104	C8.R	Right Cerebellum part 8
	105	C9.L	Left Cerebellum part 9
	106	C9.R	Right Cerebellum part 9
	107	C10.L	Left Cerebellum part 10
	108	C10.R	Right Cerebellum part 10
	109	V12	Vermis part 1 & 2
	110	V3	Vermis part 3
	111	V45	Vermis part 4 & 5
	112	V6	Vermis part 6
	113	V7	Vermis part 7
	114	V8	Vermis part 8

	115	V9	Vermis part 9
	116	V10	Vermis part 10